Correspondence to:
C. Ostle,
c.ostle@uea.ac.uk

Net community production in the North Atlantic Ocean derived from Volunteer Observing Ship data

Clare Ostle[1,2], Martin Johnson[1,3], Peter Landschützer[1,4], Ute Schuster[1,5], Susan Hartman[6], Tom Hull[1,3], and Carol Robinson[1]

[1]Centre for Ocean and Atmospheric Sciences, School of Environmental Sciences, University of East Anglia, Norwich, UK, [2]Sir Alister Hardy Foundation for Ocean Science, Plymouth, UK, [3]Centre for Environment Fisheries and Aquaculture Science, Lowestoft, UK, [4]Institute of Biogeochemistry and Pollutant Dynamics, ETH Zürich, Zürich, Switzerland, [5]College of Life and Environmental Sciences, University of Exeter, Exeter, UK, [6]National Oceanography Centre, Southampton, UK

Abstract The magnitude of marine plankton net community production (NCP) is indicative of both the biologically driven exchange of carbon dioxide between the atmosphere and the surface ocean and the export of organic carbon from the surface ocean to the ocean interior. In this study the seasonal variability in the NCP of five biogeochemical regions in the North Atlantic was determined from measurements of surface water dissolved oxygen and dissolved inorganic carbon (DIC) sampled from a Volunteer Observing Ship (VOS). The magnitude of NCP derived from dissolved oxygen measurements (NCP_{O_2}) was consistent with previous geochemical estimates of NCP in the North Atlantic, with an average annual NCP_{O_2} of 9.5 ± 6.5 mmol O_2 m^{-2} d^{-1}. Annual NCP_{O_2} did not vary significantly over 35° of latitude and was not significantly different from NCP derived from DIC measurements (NCP_{DIC}). The relatively simple method described here is applicable to any VOS route on which surface water dissolved oxygen concentrations can be accurately measured, thus providing estimates of NCP at higher spatial and temporal resolution than currently achieved.

1. Introduction

The global cycling of oxygen and carbon is regulated by the interactions between oceanic physical and biogeochemical processes including mixing and plankton respiration and photosynthesis. The solubilities of oxygen (O_2) and carbon dioxide (CO_2) are inversely proportional to temperature, so the seasonality of the saturation concentrations of these gases correlates with seasonal temperature changes [*Boyer et al.*, 1999]. The concentrations of O_2 and CO_2 are further influenced by physical processes including bubble injection [*Woolf and Thorpe*, 1991], and mixing of deep, often oxygen deplete and CO_2 replete waters into the mixed layer with associated increased nutrient concentrations stimulating biological production. Heterotrophic oxidation (respiration) leads to the production of dissolved inorganic carbon (DIC), whereas autotrophy (photosynthesis) leads to a reduction of DIC [*Falkowski*, 1998]. Improved measurements of respiration and photosynthesis and the processes that determine their variability will aid our prediction of their responses to natural and anthropogenic forcings [*Najjar and Keeling*, 2000; *Lee*, 2001].

Net community production (NCP) (in the sense of *Williams* [1993]) indicates the balance between production of organic carbon by autotrophs (*P*) and production of CO_2 by heterotrophs (*R*) at the time scale and space scale of the measurement technique used [*Serret et al.*, 2009]. The metabolic state of a system can be defined by NCP ($= P - R$), with autotrophic systems occurring when gross primary production is greater than respiration and heterotrophic systems occurring when respiration is greater than primary production [*Ducklow and Doney*, 2013].

Our study region in the North Atlantic lies between 14°N and 50°N. It is an important sink for atmospheric CO_2, with the net air-sea flux of CO_2 estimated at approximately -0.22 pg C yr^{-1} (negative value representing marine uptake from the atmosphere), representing 13% of the global contemporary carbon sink [*Gruber et al.*, 2009; *Takahashi*, 2009; *Schuster et al.*, 2013]. The CO_2 sink in the North Atlantic is maintained by year-round cooling and northward transport of waters to the Arctic. It is further accentuated by phytoplankton blooms that primarily occur within the subpolar gyre during spring [*Watson et al.*, 2009]. The North Atlantic Ocean includes regions associated with high uptake of CO_2 and productivity [*Schuster et al.*, 2013], poleward of 40°N [*Takahashi and Sutherland*, 2002], as well as oligotrophic regions associated

with low productivity [*Ducklow et al.*, 1995], such as the North Atlantic subtropical gyre. Determining the metabolic state of such regions is of key importance to determine the temporal and spatial variability in the uptake of carbon in the North Atlantic.

The North Atlantic has been sampled through repeat transects such as the Atlantic Meridional Transect and mooring sites such as the Bermuda Atlantic Time-series Study (BATS) and the European Station for Time Series in the Ocean (ESTOC) [*Robinson et al.*, 2006; *Emerson and Stump*, 2010; *Cianca et al.*, 2013]. However, there continue to be biases in the spatial and temporal coverage of data, such that oligotrophic waters are under sampled compared to shelf regions, particularly in the tropical southwestern side of the North Atlantic, and full seasonal trends are rarely recorded [*del Giorgio and Williams*, 2005; *Serret et al.*, 2006; *Quay et al.*, 2010]. Although there are a number of techniques available to derive NCP from in situ data, many of the methods are expensive and time consuming and many of the processes involved, such as those that influence gas exchange, are not yet fully constrained [*Lefèvre and Merlivat*, 2012; *Emerson and Stump*, 2010]. This has led to the continued debate surrounding the metabolic state of oligotrophic regions derived from in situ and in vitro measurements, with in vitro estimates of NCP often suggesting heterotrophy while in situ estimates consistently report autotrophy [*Williams et al.*, 2013]. These challenges mean that there are few regions in the global ocean where the current NCP rates are known [*Quay et al.*, 2010]. The aim of this study is to develop a method for estimating NCP using automated high-frequency measurements of surface water oxygen concentration collected on a Volunteer Observing Ship (VOS). We present in situ seasonal estimates of NCP between December 2011 and March 2013 within five biogeochemical regions in the North Atlantic. Our calculation of NCP involves a simple quasi-1-D box model to estimate abiotic processes that may influence oxygen concentration [*Emerson and Stump*, 2010; *Emerson*, 1987] in order to determine the biologically driven oxygen change with time. These results are compared with published in situ estimates of NCP derived from oxygen measurements and an alternative technique for the calculation of NCP, which utilizes the seasonal change in dissolved inorganic carbon (DIC) [*Bates et al.*, 2005]. This study demonstrates that well-constrained NCP estimates can be achieved through VOS campaigns, opening the way for expanded coverage of empirical NCP estimates for the global ocean.

2. Methods

2.1. Automated Sampling

Using a VOS as an oceanic measuring platform is highly efficient in terms of cost and spatial and temporal coverage. However, VOSs that are commercial ships are limiting in terms of laboratory space and have no scientific personnel on board, which means that they often depend on automated sampling systems. There are a number of methods for measuring the oxygen budget, yet many of these methods are labor intensive and costly, such as the use of Ar/O_2 ratios. Although not globally applicable due to regional variability in horizontal temperature gradients that can influence the solubility of oxygen, preliminary data collected in the Western English Channel suggest little difference between estimates of NCP derived from measurements of Ar/O_2 and those derived from optode measurements of dissolved oxygen [*Gloël*, 2012]. Several VOS routes are equipped with optodes to continuously measure surface water dissolved oxygen, but to our knowledge, these data have not yet been used to derive estimates of NCP. The VOS (MV *Benguela Stream*) used in this study operates between Portsmouth (UK) and the Caribbean Islands completing one return voyage every 28 days.

A dual oxygen/temperature sensor (Aanderaa optode, model 3835), a conductivity sensor (Aanderaa, model 3919), and a temperature sensor (Aanderaa, model 3210) are permanently installed on the MV *Benguela Stream* using the setup described by *Schuster and Watson* [2007]. The optode measures dissolved oxygen concentration based on the principle of dynamic luminescent quenching. Ambient oxygen acts as the quenching agent, and depending on the intensity and duration of red luminescence emitted after being excited by a blue-green light, the absolute oxygen concentration can be determined [*Aanderaa Data Instruments*, 2007] (see *Körtzinger et al.* [2005] for further details). Data are recorded every minute onto an instrument computer. After each voyage the raw data are returned to shore where they undergo quality control.

The in situ temperature and conductivity sensors are calibrated annually by the manufacturer and additionally monthly using a three-point temperature calibration and discrete seawater salinity samples. Calibration of oxygen measurements are described below. All raw data are recorded with concurrent

latitude, longitude, and UTC (Universal Time Coordinated) by a GPS (Global Positioning System) integrated into the instrument.

2.2. Discrete Sampling

Water samples were collected by scientific personnel on voyages in April/May 2012, June/July 2012, September/October 2012, and January/February 2013.

The ship's seawater intake is at 3–5 m below the sea surface depending on cargo loading [*Schuster and Watson*, 2007]. The seawater passes through a coarse strainer (1 mm) before entering the instruments and a T-piece. Surface seawater for chemical analysis was collected from this T-piece at the ship's sea chest using hydrostatic flow, minimizing any temperature fluctuations from the surrounding environment [*Cooper et al.*, 1998]. Tygon® tubing is connected to the T-piece in order to carefully control the flow of water into the sample bottle and check for bubbles within the tubing. Temperature (T) and conductivity of the seawater were recorded at the time of sampling. Samples were collected for dissolved oxygen, total dissolved inorganic carbon (DIC), total alkalinity (TA), salinity, nitrate, silicate, and phosphate. Dissolved oxygen, DIC, and TA samples were collected every 2 h during daylight hours. Nutrient and salinity samples were collected every 4 and 12 h, respectively. These latter samples were analyzed at the National Oceanography Centre Southampton, using a SEAL AutoAnalyzer [*Grasshoff et al.*, 1999] and a Guildline Autosal salinometer (8400B), respectively.

2.3. Winkler Analysis and Sample Storage

Dissolved oxygen samples were fixed on board using standard procedures [*Grasshoff et al.*, 1999] and stored underwater until analysis onshore. This method of storage has been found to give 100% recovery of dissolved oxygen concentration over a period of 4 months [*Zhang et al.*, 2002]. Samples were only collected on the return crossing of each voyage; therefore, the longest a sample was stored before being analyzed was 12 days. A preliminary 36 day longevity experiment showed that this storage procedure had a minimal effect on the measured oxygen concentration (< 0.01 mmol m^{-3}). Dissolved oxygen concentration was determined by Winkler titration [*Williams and Jenkinson*, 1982; *Winkler*, 1888]. Depending on sampling technique and titration method, the typical precision of Winkler titrations during fieldwork is 0.015–0.7% [*del Giorgio and Williams*, 2005]. The sodium thiosulphate titrant was calibrated with potassium iodate (Wako Pure Chemical Industries, Ltd., Osaka, Japan) to a precision of < 0.1%.

2.4. DIC and TA Analysis

The DIC and TA samples were fixed on board following standard methodology outlined in *Dickson et al.* [2007] and analyzed once back in the laboratory using the VINDTA 3C (Versatile INstrument for the Determination of Total inorganic carbon and titration Alkalinity), which combines the titration of acid to determine TA and a coulometric method for the measurement of DIC [*Mintrop*, 2011]. Routine calibration using certified reference material (CRM) (provided by A. G. Dickson, Scripps Institution of Oceanography) and corrections for silicate and phosphate enabled a precision of 1.46 mmol m^{-3} for TA and 2.55 mmol m^{-3} for DIC, calculated from the standard deviation between CRMs [*Dickson et al.*, 2007].

2.5. Data Processing and Optode Calibration

The salinity measurements derived from the conductivity probe were calibrated with measurements of salinity made with the salinometer on discrete seawater samples. The oxygen concentration derived from the optode could then be corrected to in situ salinity using equations provided in the Aanderaa operating manual [*Aanderaa Data Instruments*, 2007]. These optode-derived oxygen concentrations were calibrated with the Winkler titration data.

Winkler oxygen data were plotted against colocated 1 min averaged optode values, and Chauvenet's criterion [*Glover et al.*, 2005] was applied to remove outliers. Only one data point was removed using this method. A standard model 1 linear regression was used to determine the calibration factors with an R^2 value of 0.94 ($n = 99$); see Figure 1 [*Sokal and Rohlf*, 1995].

This optode calibration (see Figure 1) was applied to all of the optode measurements made during the study period, as it was found to be consistent, and avoids any seasonal bias that may be introduced using cruise-specific regressions. The error of this calibration was calculated as the RMSE (root-mean-square error) of the difference between the measured Winkler oxygen and the oxygen predicted by the regression (RMSE residuals = 4.3 mmol m^{-3}, percentage error of the mean = 1.7%).

$$O_2 \text{corrected} = O_2 \text{optode} * 1.5 - 74$$

$$R^2 = 0.94$$
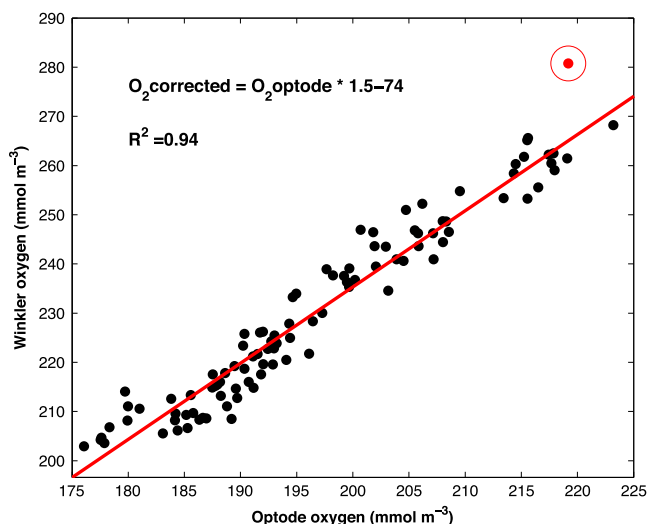
Figure 1. Property-property plot of Winkler-derived oxygen concentration against optode-derived oxygen concentration (filled black circles) showing the standard model 1 linear regression line (red line), correction equation for optode oxygen, and its R^2. A single outlier was identified (filled red circle) and excluded from the oxygen calibration.

During February 2012 there were sporadic temperature shifts during sections of the voyage that affected the oxygen concentration recorded by the optode. This was attributed to a technical fault, and these data were removed during the quality control process.

The uncertainty of our oxygen measurements was calculated using a combination of the percentage error from the RMSE of the residuals (1.7%), an estimate of the error associated with the underway sampling method (1%), and the precision determined with the standard iodate solution (0.1%), which gives a total error of ±2.8%.

2.6. Biogeochemical Regions

The study area was divided into biogeochemical regions in order to assess the spatial variability in NCP in the midlatitude North Atlantic under different biogeochemical regimes. The method used for the division of these regions is similar to that of *Hooker et al.* [2000], whereby the second derivative of in situ *T*, in situ density, and satellite-derived natural logarithm of chlorophyll *a* (Chl *a*) (Moderate Resolution Imaging Spectroradiometer (MODIS) Aqua level 3 standard chlorophyll product, http://oceandata.sci.gsfc.nasa.gov) [*Sharqawy*, 2010] were calculated along the ship tracks. The second derivatives for each parameter were normalized to ensure equal weighting and then averaged. Peaks in these averaged second derivatives identified the latitudinal boundaries between each biogeochemical region (see Figure 2). This method was chosen in preference to using static ecologically defined provinces such as *Longhurst* [2006], because this allows the dynamics of the boundaries to shift from year to year defined by in situ and satellite observations.

This method identified four peaks, thereby dividing the study area into five biogeochemical regions, labeled 1 to 5 from north to south (see Figure 2). These dynamic biogeochemical regions were used throughout
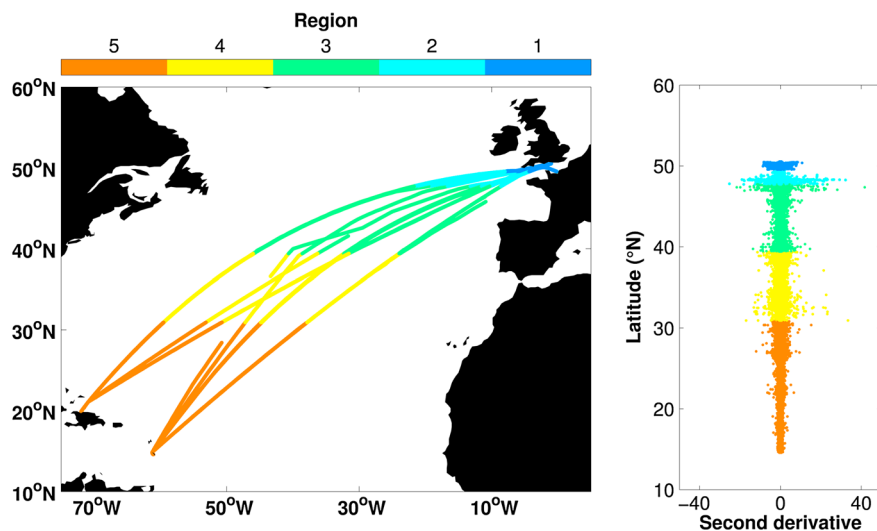
Figure 2. Map of the midlatitude North Atlantic, divided into five biogeochemical regions. The dynamic latitudinal boundaries of which are defined by peaks in the second derivative of *T*, density, and Chl *a*. The overlapping ship tracks of 16 voyages between December 2011 and March 2013 are shown.

the study as they avoid calculating NCP across different water masses as the ship moved and biases associated with the changing latitude of the ships tracks. These biogeochemical regions are in broad agreement with ecologically defined provinces within the North Atlantic [*Longhurst*, 2006; *Hooker et al.*, 2000], with regions 1 to 5 aligning approximately with the *Longhurst* [2006] biogeochemical provinces NECS (Northeast Atlantic Coastal Shelves), NECS/NADR (North Atlantic Drift), NADR/NASE (North Atlantic Subtropical East), NASW (North Atlantic Subtropical West), and NASW/NATR (North Atlantic Tropical), respectively.

2.7. Calculation of NCP$_{O_2}$

Net community production was derived from the change in the inventory of oxygen in the surface ocean with time [*Emerson*, 1987; *Emerson and Stump*, 2010] (NCP$_{O_2}$, mmol O_2 m^{-2} d^{-1}). The corrected continuous surface measurements collected between December 2011 and March 2013 were divided into biogeochemical regions (see Figure 2), and monthly means for each region were calculated for calibrated dissolved oxygen, temperature, and salinity.

NCP$_{O_2}$ was calculated as the biological component ($\Delta O_2 Bio$, mmol m^{-3}) of the total change in oxygen concentration within the mixed layer (h, m) over the period between monthly observations (Δt, days).

$$\text{NCP}_{O_2} = h \frac{\Delta O_2 \text{Bio}}{\Delta t} \tag{1}$$

$\Delta O_2 Bio$ was determined from the difference between the observed changes in dissolved oxygen ($\Delta O_2 Obs$, mmol m^{-3}) and those predicted from abiotic ($\Delta O_2 Abio$, mmol m^{-3}) processes (i.e., solubility, gas exchange, and changes in the mixed layer depth) on a monthly basis.

$$\Delta O_2 \text{Bio} = \Delta O_2 \text{Obs} - \Delta O_2 \text{Abio} \tag{2}$$

Where $\Delta O_2 Bio$, $\Delta O_2 Obs$, and $\Delta O_2 Abio$ are in units of mmol m^{-3}.

$\Delta O_2 Abio$ is calculated using the ordinary differential equation solver 45 in MATLAB [*Glover et al.*, 2005]. Temperature (T, °C) and mixed layer depth (MLD) (h, m) are assumed to vary linearly over the integration period. Monthly mean MLD was calculated for each region using ECCO2 daily 0.25° MLD [*Menemenlis et al.*, 2008]. Wind speed (U, m s^{-1}) was applied as a time-variable input obtained from European Centre for Medium-Range Weather Forecasts 6-hourly 0.75° 10 m wind speed [*Uppala et al.*, 2005]. Monthly below-thermocline oxygen concentrations ($O_2 Deep$, mmol m^{-3}) were derived from the World Ocean Atlas 2009 climatology [*Garcia et al.*, 2010] by taking the mean oxygen concentration from 0 to 25 m below the MLD within each region. $O_2 Deep$ remains constant within each NCP integration period. The predicted abiotic oxygen concentration change was computed as the sum of entrainment (E) and the flux of oxygen between the atmosphere and the ocean (FO_2) over the mixed layer (h) on a daily time step within the solver (dt).

$$\Delta O_2 \text{Abio} = \int_0^{\Delta t} \frac{(E + FO_2)}{h} \times dt \tag{3}$$

Therefore, $\Delta O_2 Abio$ is the predicted physical change in oxygen concentration over the period between monthly observations, due to E and FO_2. This method can be described as a quasi-1-D (vertical) box model applied over monthly integrations in each of the biogeochemical regions.

2.7.1. Entrainment

When the mixed layer deepens over time, the oxygen concentration will change due to mixing between surface and deep waters. When the mixed layer shoaled, we assumed that this did not cause a change in oxygen concentration. E is calculated as described in equation (4).

$$\text{if } \frac{dh}{dt} > 0; E = \frac{dh}{dt} \times (O_2 \text{Deep} - O_2) \tag{4}$$

Where O_2 is the oxygen concentration at the beginning of each solver time step.

2.7.2. O_2 Exchange With the Atmosphere

FO_2 is calculated following *Woolf and Thorpe* [1991], where the standard thin film model of gas exchange is combined with a term to account for the transient supersaturation due to bubble injection. The transfer velocity, kO_2, and the concentration terms are expressed in terms of a concentration gradient on the water side of the interface:

$$FO_2 = kO_2 \times ((O_2Sol \times BO_2) - O_2) \tag{5}$$

Where O_2Sol, mmol m^{-3} is the oxygen solubility (or saturation) concentration (i.e., the seawater concentration that would be in equilibrium with an assumed atmospheric concentration of 0.2095 atmospheres of oxygen) calculated using the MATLAB function O2sol.m (Copyright©2010, eMarine Information Infrastructure (eMII) and Integrated Marine Observing System (IMOS). All rights reserved.). This function utilizes the equations outlined in *García and Gordon* [1992], which are based on values obtained from *Benson and Krause* [1984]. O_2Sol was determined using in situ temperature and salinity measured at the same time, geographic location, and depth as the optode measurement. BO_2 is the functional increase in saturation due to bubble injection [*Woolf and Thorpe*, 1991]. More recent bubble parameterizations based on models and observations exist but deviate from one another at high wind speeds (> 10 m s^{-1}) [*Stanley et al.*, 2009; *Liang et al.*, 2013]. The NCP estimates were found to be relatively insensitive to the supersaturation bubble term, so the empirically derived model of *Woolf and Thorpe* [1991] was deemed most appropriate.

$$BO_2 = 1 + 0.01 \times (\frac{U}{U_O})^2 \tag{6}$$

Where U_O is the wind speed at which the oxygen saturation is supersaturated at 101%; this is a constant given as 9 m s^{-1} [*Woolf and Thorpe*, 1991]. The wind speeds used for equation (6) were the average wind speed within each biogeochemical region for the 6 h period preceding each solver time step to account for the instantaneous effect of varied wind speeds on bubbles.

Waterside transfer velocity, kO_2, was calculated using *Wanninkhof et al.* [2009] which represents the different wind speed regimes as polynomial equations, from purely diffusive flux through linear (smooth surface), quadratic (rough surface), and cubic (bubble-mediated) regimes.

$$kO_2 = 0.24 \times ((3 + 0.1U + 0.064U^2 + 0.011U^3) \times (\frac{ScO_2}{660})^{-0.5}) \tag{7}$$

Where kO_2 is in m d^{-1}, U is the daily averaged wind speed in m s^{-1}, and ScO_2 is the temperature-dependent Schmidt number of oxygen [*Keeling and Stephens*, 1998]:

$$ScO_2 = 1638 - 81.83T + 1.483T^2 - 0.008004T^3 \tag{8}$$

Due to variable 6-hourly winds within the solver time steps, square and cubic means were calculated prior to daily averaging to avoid issues with nonlinearity [*Wanninkhof et al.*, 2009].

2.8. Calculation of NCP$_{DIC}$

Net community production can also be derived from seasonal changes in the concentration of DIC (NCP$_{DIC}$, mmol C m^{-2} d^{-1}) within the surface layer [*Williams*, 1993; *Bates et al.*, 2005; *Mathis et al.*, 2010]. This method assumes that changes in DIC caused by processes other than NCP (e.g., air-sea CO_2 gas exchange, advection, precipitation, evaporation, formation and dissolution of calcium carbonate, riverine inputs, vertical diffusion, and entrainment) can either be accounted for or are assumed to be negligible [*Bates et al.*, 2005].

The influence of advection was estimated from the regional change in TA between seasons. TA is not affected significantly by photosynthesis and respiration; therefore, a change in TA is likely caused by advection and/or entrainment. As there were only small changes in observed TA between seasons (mean change < 0.1 mmol m^{-3} d^{-1}), we assumed that the effect of advection on the seasonal change in DIC was negligible [*Lefèvre and Merlivat*, 2012].

To remove the impact of changes in local precipitation and evaporation [*Bates et al.*, 2005], DIC was normalized to a salinity of 35 (*n*DIC), resulting in a mean decrease in DIC of 69 mmol m^{-3}.

Table 1. Error Associated With Each Input Variable Used to Calculate NCP_{O_2} and NCP_{DIC}

Variable	Error	Reference/Method
O_2Obs	±2.8%	Combination of RMSE of residuals (1.7%), underway sampling method (1%), and method accuracy from the iodate standard (0.1%)
O_2Deep	±4.4661 (mmol m^{-3})	0.1 (mL L^{-1}) Standard error of the mean [*Garcia et al.*, 2010]
Salinity (S)	±0.05	Calculated from temperature and conductivity, calibrated using discrete salinity samples
Temperature (T)	±0.03 (°C)	Aanderaa 3210 sensor accuracy
MLD (h)	±30%	*von Allmen et al.* [2009]
Wind Speed (u)	±1.1 (m s^{-1})	*Stoffelen* [1996]
kO_2	±30%	*M. Johnson* [2010]
DIC	±2.55 (mmol m^{-3})	Mean standard deviation of CRM DIC
TA	±1.46 (mmol m^{-3})	Mean standard deviation of CRM TA
NO_3	±0.1 (mmol m^{-3})	SEAL Auto Analyzer accuracy from international standards

Riverine input is likely to only affect those regions that are closest to the coast, i.e., region 1; insufficient data were available to calculate NCP_{DIC} in this region, and riverine input can be assumed to be negligible for the other regions.

To account for the formation and dissolution of calcium carbonate, a correction factor was used, of half the temporal change in TA, after adjusting this for the temporal change in NO_3 [*Lee*, 2001; *Mathis et al.*, 2010]:

$$\text{Corr} = \frac{(TA^{t1} - TA^{t2})}{\Delta t} + \frac{(NO_3^{t1} - NO_3^{t2})}{\Delta t} \times 0.5 \tag{9}$$

Where $(TA^{t1} - TA^{t2}/\Delta t)$ is the seasonal change of TA between time 1 ($t1$) and time 2 ($t2$), $(NO_3^{t1} - NO_3^{t2}/\Delta t)$ is the seasonal change in NO_3 for the same time period, and Δt is the number of days between $t1$ and $t2$.

NCP_{DIC} was determined for each of the five biogeochemical regions as the change in nDIC over time across the mixed layer (h, m), corrected for the formation and dissolution of calcium carbonate:

$$NCP_{DIC} = h\frac{(n\text{DIC}^{t1} - n\text{DIC}^{t2})}{\Delta t} - \text{Corr} \tag{10}$$

Where $(n\text{DIC}^{t1} - n\text{DIC}^{t2}/\Delta t)$ is the seasonal change in nDIC. We chose the spring for $t1$ and the autumn for $t2$; the autumn values were chosen rather than the summer values because there was little to no change in nDIC between the spring and the summer.

2.9. Photosynthetic Quotient
The photosynthetic quotient (PQ) was calculated as the ratio between the two independent estimations of NCP:

$$PQ = \frac{NCP_{O_2}}{NCP_{DIC}} \tag{11}$$

2.10. Uncertainty
The RMSE was calculated for each of the input variables in each of the regions using a Monte Carlo approach (see Table 1 for individual errors) [*Quay et al.*, 2010].

The RMSE was first calculated separately for errors above and below the mean NCP as variables contributed differently and then combined using the root sum square error to give the variance from the mean NCP over a period of time (i.e., seasonal error and annual error). The errors are different in each region due to the varying geographical impacts of the input variables. For example, region 3 had the largest error associated with its seasonal and annual NCP_{O_2} values due to the sharp change in oxygen saturation that occurred between January and February in 2012 (see Figure 3).

To account for the error and potential bias of excluding CO_2 exchange in our NCP_{DIC} calculation, we have estimated the likely CO_2 flux between spring and autumn for each region using a neural network-based
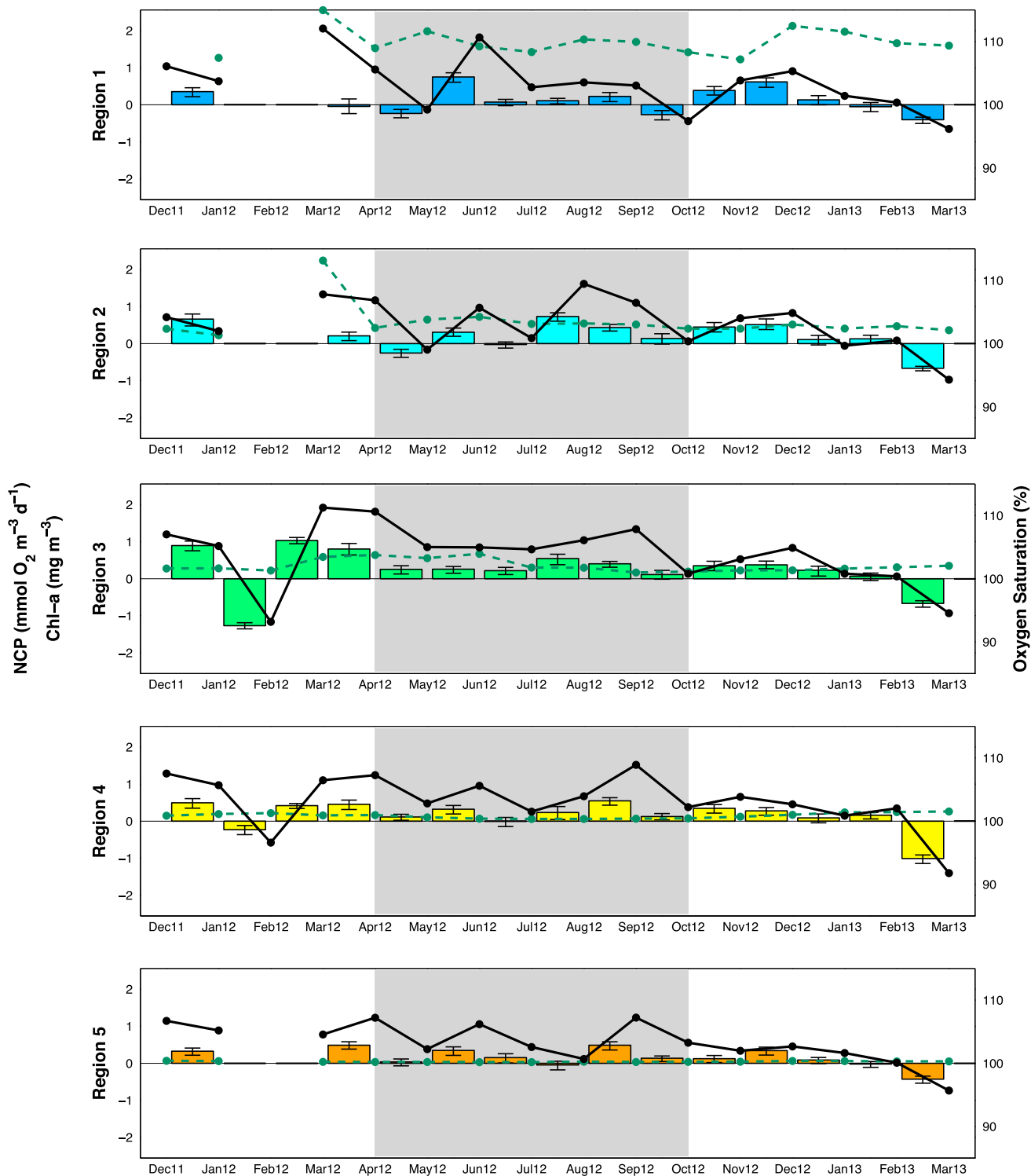
Figure 3. Monthly mean NCP$_{O_2}$, Chl a, and oxygen saturation over time in each of the five biogeochemical regions (see Figure 2). Monthly NCP$_{O_2}$ data were calculated using equations (1)–(8) and are shown as colored bars with error bars indicating the uncertainty ((mmol O$_2$ m^{-3} d^{-1}), left axis); monthly Chl a data are shown as green filled circles and dashed line ((mg m^{-3}), left axis); and oxygen saturation are represented by the black closed circles and line ((%), right axis). The grey area is the period from which the summer mean NCP$_{O_2}$ was estimated.

Table 2. Error Associated With the Air-Sea Flux of CO_2[a]

Region	CO_2 Flux (mmol m^{-2} d^{-1})	IAV CO_2 Flux[b] (mmol m^{-2} d^{-1})	MLD (m)	Error From Carbon Uptake (%)	Error From IAV (%)
1	4.66	0.88	25.16	NA[c]	NA[c]
2	4.96	0.77	50.80	30.72	4.83
3	3.75	0.36	49.19	21.50	1.98
4	0.79	0.66	64.30	4.01	3.33
5	0.03	0.36	44.01	0.39	6.08

[a]Average CO_2 flux estimates from April to October are derived from *Landschützer et al.* [2014], and mixed layer depths are derived from *Menemenlis et al.* [2008].
[b]Calculated as 1 standard deviation of the interannual variability (IAV) in CO_2 flux.
[c]Insufficient DIC and TA data were available in spring 2012 within this region; therefore, a NCP$_{DIC}$ estimate was not calculated; hence, no error estimate. NA = not available.

monthly climatology (from the years 1998–2011) of the ocean carbon sink [*Landschützer et al.*, 2014]. We cannot assume the same fast equilibration times for carbon as we do for oxygen; hence, we account for the exchange of CO_2 as a result of the disequilibrium between the atmosphere and surface ocean CO_2 partial pressures by incorporating the CO_2 flux into our uncertainty. Ocean carbon uptake was calculated per unit volume by dividing the air-sea CO_2 flux by the mean summer ECCO2 MLD [*Menemenlis et al.*, 2008] within each region. As these regions are normally sinks for CO_2 during this time of year, this introduces a negative bias into our NCP$_{DIC}$ estimates (i.e., unaccounted for CO_2 influx to the surface ocean leads to an underestimation in biological CO_2 uptake; see Table 2). As there are no estimates of CO_2 flux from *Landschützer et al.* [2014] for the study year, to estimate the possible effect of 2012 being an atypical year, we considered the interannual variability (IAV) in annual CO_2 flux in the climatology (taken as 1 standard deviation) for each region (Table 2) and included this in our error estimation. Negative error bars are thus the sum of measurement uncertainty and any net negative excursion of the uncertainty from the climatological mean CO_2 flux (i.e., representing a possible net release of CO_2 into the atmosphere over the period of NCP$_{DIC}$ calculation. Negative uncertainty from the climatological mean only exceeds measurement uncertainty in region 5 where the percentage error from interannual variability is greater than the climatological CO_2 flux; see Table 2.). Positive error bars are the sum of measurement uncertainty and any net positive flux, i.e., a net sink of CO_2 from the atmosphere into the surface mixed layer over the period of NCP$_{DIC}$ calculation.

2.11. Assumptions and Limitations

Due to lack of DIC measurements and the different residence times of oxygen and carbon dioxide [*Sarmiento and Gruber*, 2006], the calculation of NCP$_{DIC}$ is more simplistic than that of NCP$_{O_2}$ and the uncertainties associated with the calculation are therefore less easy to estimate; see section 2.10. Our calculation of NCP$_{DIC}$ does not take into account the additions of DIC through gas exchange, vertical diffusion, and entrainment. These generally increase as the season progresses, which can lead to an underestimation in NCP$_{DIC}$ [*Mathis et al.*, 2010]. This was suggested by our estimations of the carbon uptake, as all five regions were found to be net sinks of CO_2 over the summer period, thus increasing the positive error on our NCP$_{DIC}$ estimates (Table 2).

Horizontal advection and vertical diffusion (diapycnal and isopycnal) were necessarily neglected in our calculations due to the lack of available measurements. However, as these have been shown to have a relatively small influence on oxygen concentration due to the rapid equilibration of oxygen with the atmosphere, this is unlikely to be a significant omission [*Emerson et al.*, 2008; *Lefèvre and Merlivat*, 2012]. Entrainment was not incorporated into the NCP$_{DIC}$ calculation as no observational depth distribution DIC data were found within 1° latitude × 1° longitude during the same month (independent of the sample year) of the sampling routes. Until more data of DIC depth distributions become available (such as in the updated Global Ocean Data Analysis Project [*Key et al.*, 2004] data set, whose release is imminent), such analysis will be difficult or impossible in many regions of the global ocean. *Lee* [2001] estimates that in the North Atlantic (between 40°N and 70°N) and the mid-Atlantic (40°N and 40°S) about 2.8% and 11.9% (respectively) of the estimate of NCP from the summer change in DIC are accounted for by diffusive carbon flux. However,
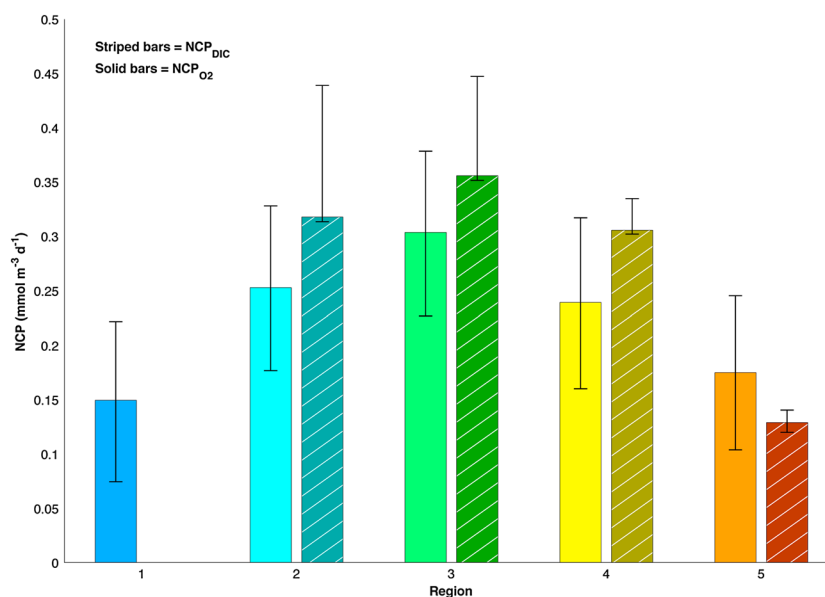
Figure 4. Summer mean NCP_{O_2}, and NCP_{DIC}, in each of the five biogeochemical regions (see Figure 2) between spring and autumn 2012. The darker-colored striped bars represent the NCP_{DIC}, and the lighter-colored solid bars represent the NCP_{O_2}, and the error bars indicate uncertainties identified for each. Note that in region 1, insufficient data could be collected for NCP_{DIC} in spring 2012 and that there is a negative bias in the NCP_{DIC} estimates associated with CO_2 flux (see section 2.10).

as there was no significant change in TA throughout the summer sampling period, this suggests that DIC had not been entrained from below the mixed layer [*Lefèvre and Merlivat*, 2012], and vertical diffusion and horizontal transport are likely to have only contributed in a minor way [*Gruber et al.*, 2002].

Entrainment was incorporated into the NCP_{O_2} calculations by using climatological oxygen depth distributions and a mixed layer reanalysis. The large error associated with these products (see Table 1) significantly influences the error on our NCP_{O_2} estimates. This influence is increased when calculating NCP per unit area rather than per unit volume due to the high error associated with the multiplication across the mixed layer depth (equations (1) and (10)). We estimate that the average error on our annual estimate of NCP_{O_2} (mmol m^{-2} d^{-1}) is increased by 15.75% due to the uncertainty on the entrainment terms. As we only have surface measurements, we cannot constrain potential systematic bias in the data products and climatology used; however, we assume that any possible bias is incorporated in the large uncertainty associated with these products.

3. Results

3.1. Seasonal Cycle of NCP_{O_2}

Monthly mean NCP_{O_2} was calculated for each month between December 2011 and March 2013 for each biogeochemical region shown in Figure 2, from the daily time step quasi-1-D model and the calculations described above (see equations (1)–(8)), and is shown in Figure 3 together with mean monthly Chl *a* data (obtained from Aqua-MODIS at a resolution of 9 km and frequency of 1 month, http://oceandata.sci.gsfc.nasa.gov) and oxygen saturation.

Surface dissolved oxygen remains supersaturated for most of the sampling period. A distinct decrease in oxygen saturation occurs in February 2012 in regions 3 and 4, followed by supersaturation in March 2012. This change in saturation state occurs at the time of rapid shoaling of the mixed layer depth, which is often associated with the onset of primary production [*Sverdrup*, 1953]. Unfortunately, during this time there were sporadic electrical faults within the sampling setup. As a result, data are missing from regions 1, 2, and 5 for these months; however, the same trend can be seen in all five regions between February and March 2013, with the saturation state becoming undersaturated in March. This suggests that a similar trend may have been present in the months where data are missing. Throughout the rest of the time series, the oxygen saturation is mostly supersaturated within each region, except for times of undersaturation that occur within

Table 3. Comparison of NCP and PQ Estimates

Region	NCP_{DIC} (mmol C m^{-3} d^{-1})	NCP_{O_2} (Summer) (mmol O_2 m^{-3} d^{-1})	PQ Value	Annual NCP_{O_2} (mmol O_2 m^{-3} d^{-1})[a]	Annual NCP_{O_2} (mmol O_2 m^{-2} d^{-1})[a]
1	NA[b]	0.15 ± 0.075[c]	NA[b]	0.18 ± 0.010[c]	7.1 ± 5.5[c]
2	0.32 ± 0.12[c]	0.25 ± 0.076[c]	0.80 ± 0.39[d]	0.26 ± 0.094[c]	12 ± 6.9[c]
3	0.36 ± 0.091[c]	0.31 ± 0.077[c]	0.85 ± 0.35[d]	0.27 ± 0.10[c]	9.5 ± 9.4[c]
4	0.31 ± 0.029[c]	0.24 ± 0.079[c]	0.78 ± 0.31[d]	0.22 ± 0.10[c]	10 ± 6.8[c]
5	0.13 ± 0.012[c]	0.18 ± 0.071[c]	1.4 ± 0.62[d]	0.21 ± 0.083[c]	8.7 ± 3.9[c]

[a]Estimating NCP per unit area introduces increased error associated with the MLD (section 2.11); both units have been presented here for ease of comparison with previous studies.
[b]Insufficient DIC and TA data were available in spring 2012 within this region, so neither NCP_{DIC} nor a PQ could be calculated. NA = not available.
[c]Although an error for above and below the mean NCP_{DIC} and NCP_{O_2} was calculated, the largest of these two errors is shown here.
[d]The PQ uncertainty was calculated using the minimum and maximum values within the error distribution of both NCP_{DIC} and NCP_{O_2}, and the largest of these two errors is shown here.

region 1 in May and October 2012 and in region 2 in May 2012 and January 2013. As expected, the seasonal cycle of NCP_{O_2} generally follows the seasonal cycle of oxygen saturation.

3.2. Summer Mean and Annual Mean NCP

The summer mean NCP_{O_2} for each region were calculated as the mean NCP_{O_2} between spring and autumn 2012 and are presented in Figure 4 together with the NCP_{DIC} (calculated between spring and autumn 2012; see section 2.8). There are insufficient DIC and TA data for region 1 during spring of 2012, so NCP_{DIC} for region 1 could not be calculated. The photosynthetic quotient (see equation (11)) was calculated for each region where both NCP_{DIC} and NCP_{O_2} were available. These data are presented in Table 3.

The summer means of NCP_{O_2} and NCP_{DIC} are not significantly different in all four regions where both estimates were calculated (Figure 4) and follow the same regional trend with region 3 having the highest NCP and regions 1 and 5 the lowest. As the error bars on the NCP estimates do not account for all of the assumptions of the calculations (see section 2.10 and 2.11), we can assume that the NCP estimates using the two different techniques in all four regions are not significantly different.

The annual NCP_{O_2} for each region was determined as the mean NCP_{O_2} of all 12 months in 2012. These data are compared with annual NCP_{O_2} estimates from similar geochemical studies in Figure 6.

4. Discussion

4.1. Seasonality of NCP_{O_2}

Our results show that autotrophy dominates our study area, including the western tropical and subtropical regions, with only 5 months between December 2011 and March 2013 showing negative NCP_{O_2}. This is in line with published NCP rates derived from in situ measurements, such as the study of *Neuer et al.* [2007] which found that at ESTOC between 1994 and 2000 monthly NCP values were always autotrophic. However, this contrasts with NCP estimates derived from in vitro measurements within tropical regions of the North Atlantic which are generally heterotrophic [*Williams et al.*, 2013].

Region 1 has the highest concentration of Chl *a* with peaks occurring in March, May, August, and December 2012. This seasonal cycle of Chl *a* in region 1 is observable in the oxygen saturation and in NCP_{O_2}, with NCP_{O_2} peaking between May and June as well as between November and December of 2012. The monthly range in magnitude of NCP_{O_2} decreases from region 1 to region 5 in line with a decrease in Chl *a* concentrations. Regions 4 and 5 are oligotrophic, associated with low nutrient conditions and the dominance of smaller-sized phytoplankton [*Ducklow et al.*, 1995].

Figure 5 shows for each of our five biogeochemical regions the relative contributions of various processes involved in the calculation of NCP_{O_2} (specifically, equations (2) and (3)) and how this contribution varies between regions. The seasonal pattern in gas exchange is shown in Figure 5b with sea surface outgassing of oxygen during the summer months when the mixed layer is supersaturated with oxygen and influx of oxygen into the mixed layer when it is undersaturated with oxygen in the winter months. This change
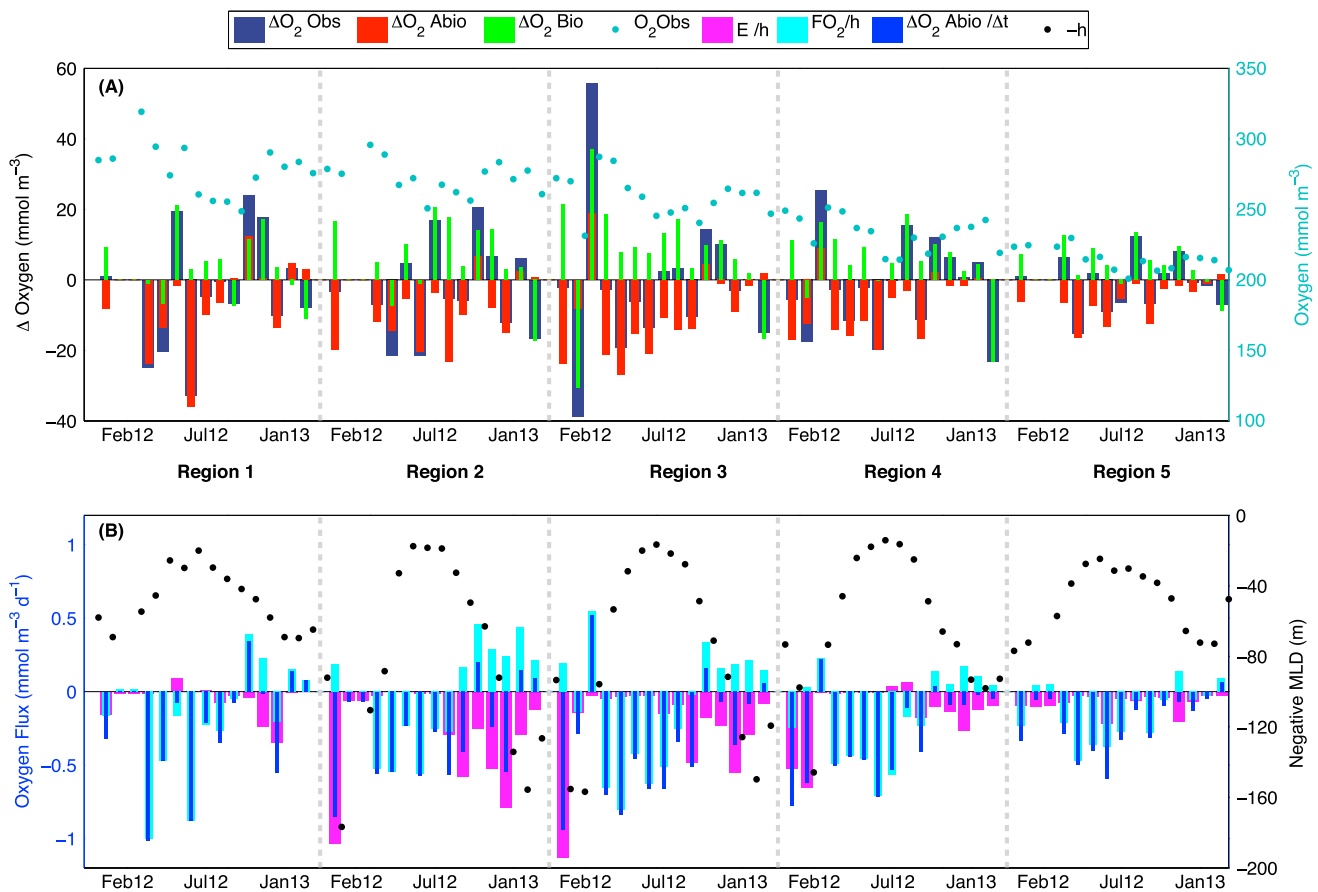
Figure 5. (a) The month-to-month change in the observed oxygen concentration ($\Delta O_2 Obs$, dark blue bars) along with the modeled abiotic and biotic contributions ($\Delta O_2 Abio$ (red bars) and $\Delta O_2 Bio$ (green bars), all in mmol m^{-3}, left axis) and the monthly oxygen concentration ($O_2 Obs$, (mmol m^{-3}), turquoise circles, right axis) from December 2011 to March 2013 in each of the five biogeographical regions. (b) The oxygen flux ((mmol m^{-3} d^{-1}), left axis) associated with entrainment (E/h, pink bars), gas exchange (FO_2/h, cyan bars), and $\Delta O_2 Abio/\Delta t$ (blue bars) between months, and the monthly negative MLD ($-h$, (m), black circles, right axis) from December 2011 to March 2013 in each of the five biogeographical regions.

from outflux to influx of oxygen occurs after July when the wind speed starts to increase and the oxygen saturation decreases. The gas exchange term generally varies in the opposite sense to the entrainment term, as the increased deepening of the mixed layer depth during the winter months causes the decrease in oxygen concentration within the mixed layer as oxygen depleted waters are entrained, while the gas exchange causes an increased oxygen concentration as the undersaturated waters are taking up oxygen from the atmosphere (Figure 5b). During most of the sampling period the oxygen concentration below the thermocline is lower than that within the mixed layer. However, during May in region 1 and briefly in July in region 4, the oxygen concentration is higher below the thermocline than within the mixed layer. These subthermocline higher concentrations of oxygen are likely due to production of O_2 by phytoplankton below the mixed layer which cannot then escape to the atmosphere [*Emerson et al.*, 2008]. The entrainment term has the largest influence in region 2 (see Figure 5b) and less of an impact in regions 1 and 5 where the mixed layer depth is shallower and there is less of a change in the mixed layer depth during the sampling period. The oxygen concentration ($O_2 Obs$) increases from region 5 to region 1 (Figure 5a), a geographical pattern that is strongly linked to decreased solubility with increasing temperatures toward the tropics [*Garcia and Keeling*, 2001]. The latitudinal pattern in the biological oxygen flux ($\Delta O_2 Bio$) shows highest values in region 3, decreasing toward regions 1 and 5.

4.2. Comparison of Two Independent NCP Estimates

The PQs for each region are given in Table 3 along with the regional mean annual NCP$_{O_2}$ for 2012. The Redfield ratio of O_2:DIC (138:106) is 1.3 [*Redfield*, 1963]; however, *Laws* [1991] suggests using PQ values of 1.4 and 1.1 for new and recycled production, respectively. Our PQ values range from 0.78 ± 0.31 in region
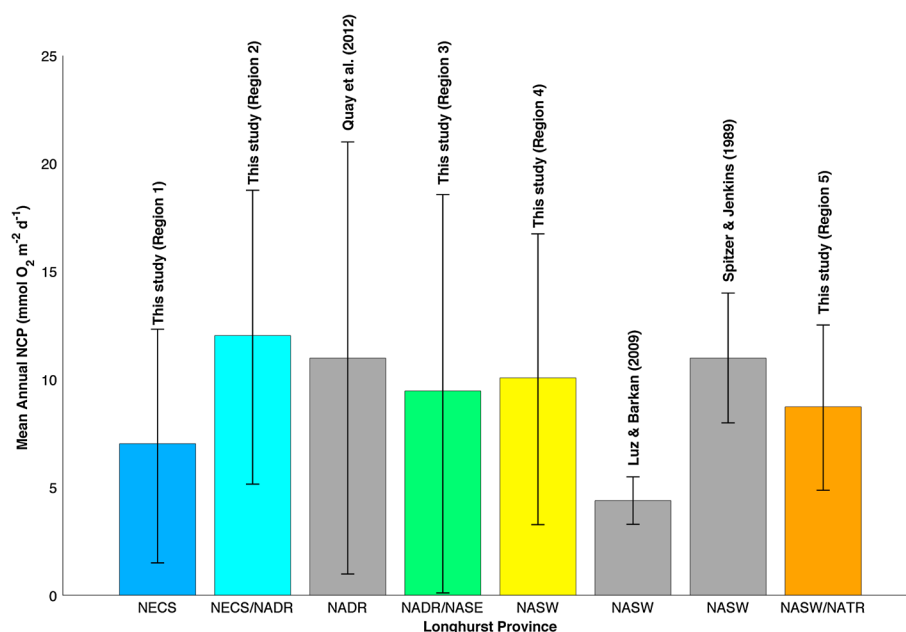
Figure 6. Mean annual NCP and their uncertainties in different biogeochemical regions in the midlatitude North Atlantic. Shown are annual mean NCP_{O_2} in each of the five biogeochemical regions obtained in this study (colored bars; see Figure 2), along with previously published mean annual NCP estimates from the North Atlantic (grey bars) [*Longhurst*, 2006].

4 to 1.4 ± 0.62 in region 5. *Lefèvre and Merlivat* [2012] measured NCP using carbon and oxygen at the Prediction and Research Moored Array in the Tropical Atlantic site and also found that NCP derived from dissolved oxygen concentrations was lower than that predicted from NCP_{DIC} and a PQ of 1.4. Published PQ values range from 0.77 ± 0.28 to 1.26 ± 0.66 [*Lefèvre and Merlivat*, 2012; *Lefèvre et al.*, 2008; *K. Johnson*, 2010] confirming that a constant value of 1.4 is not always applicable.

The calculation of NCP_{DIC} using the seasonal carbon mass balance approach makes several assumptions in that it does not take into account additions of DIC through gas exchange, vertical diffusion and entrainment, and the influence of riverine inputs (section 2.11). Although these limitations are likely to have caused an underestimation in NCP_{DIC}, our relatively low PQ values suggest that this underestimation is small.

4.3. Annual Net Community Production

The summer mean NCP_{O_2} for the months between spring and autumn is highest in region 3 and lowest in regions 1 and 5 (see Figure 4). However, the annual mean NCP_{O_2} is highest for region 2 and lowest for regions 1 and 5, (see Table 3) highlighting the intraannual variability in NCP_{O_2} within regions. It is also important to note that our annual NCP_{O_2} estimates integrate to the winter mixed layer depth, which varies considerably between regions from <100 m in regions 1 and 5 to ~150 m in regions 2, 3, and 4 (Figure 5). *Körtzinger et al.* [2008] demonstrate that at the Porcupine Abyssal Plain site, which lies within region 2, one third of the organic matter that is exported during the summer is returned to the mixed layer the following winter due to entrainment. This could explain why the regional variability seen in the summer mean NCP (higher NCP in regions 2, 3, and 4 than in 1 and 5 (Figure 4)) is not seen in the annual mean NCP_{O_2} (Figure 6).

Our estimates of annual NCP_{O_2} range from 7.1 ± 5.5 to 12 ± 6.9 (mmol O_2 m^{-2} d^{-1}) and are not significantly different from published estimates of NCP derived from geochemical oxygen budgets made in the midlatitude North Atlantic that range from 4.4 ± 1.1 to 11 ± 10 (mmol O_2 m^{-2} d^{-1}) [*Spitzer and Jenkins*, 1989; *Luz and Barkan*, 2009; *Quay et al.*, 2012]. Our study estimated an annual NCP of 12 ± 6.9 (mmol O_2 m^{-2} d^{-1}) for region 2, which falls within the *Longhurst* [2006] provinces NECS and NADR, and 9.5 ± 9.4 for region 3, which falls within the *Longhurst* [2006] provinces NADR and NASE. The geographically closest annual NCP estimate of 11 ± 10 (mmol O_2 m^{-2} d^{-1}) was derived from the CARINA (CARbon dioxide IN the Atlantic Ocean) surface O_2 data by *Quay et al.* [2012] using Ar/O_2 ratios in the *Longhurst* [2006] provinces

NADR/ARCT and SARC. *Luz and Barkan* [2009] calculated annual NCP at BATS in 2000 to 2001 using Ar/O_2 ratios, and *Spitzer and Jenkins* [1989] derived NCP at BATS in 1985 to 1986 from surface ocean O_2 mass balance. These estimates of 4.4 ± 1.1 and 11 ± 3 (mmol O_2 m^{-2} d^{-1}) respectively fall within the NASW *Longhurst* [2006] province. Our estimate of annual NCP in the NASW of 10 ± 6.8 (mmol O_2 m^{-2} d^{-1}) is similar to that of *Spitzer and Jenkins* [1989], despite the suggestion of significant interannual variability in the air-sea oxygen flux in the North Atlantic [*McKinley*, 2000]. Interestingly, our estimates of annual NCP_{O2} in the midlatitude North Atlantic are not significantly different from geochemical estimates of NCP in the North Pacific [*Emerson et al.*, 1997, 2008; *Quay et al.*, 2010].

The lack of latitudinal variability in our data agrees with the conclusions of *Emerson* [2014] and *Emerson and Bushinsky* [2014], who showed that the latitudinal variability in in situ-derived NCP estimates is often less than that in model-derived estimates of annual NCP. Global circulation models and satellite-derived models (vertically generalized productivity model) [*Behrenfeld and Falkowski*, 1997; *Najjar et al.*, 2007] give zonally averaged estimates of annual NCP in the subtropics (equivalent to our region 5) that are about half of the annual NCP in transition regions (equivalent to our regions 3 and 4) [*Emerson*, 2014]. Further in situ measurements are therefore required to determine the latitudinal and interannual variability in NCP and investigate the processes or assumptions that may cause in situ and model estimates of NCP to differ. *Emerson and Bushinsky* [2014] and *Körtzinger et al.* [2005] propose a technique using atmospheric pO_2 to correct the drift of optodes installed on Argo and other profiling floats. The next step is to design an automated and accurate way of correcting for optode drift on VOSs potentially by using measurements of atmospheric pO_2. This would enable accurate automated surface oxygen measurements and hence NCP on a global scale.

5. Summary

We present the first estimates of mean annual NCP for five biogeochemical regions within the midlatitude North Atlantic, covering approximately 4,300,000 km^2. We developed a simple and cost-effective method (in terms of personnel time and shipboard space requirements) which is therefore applicable for use on VOSs. The method was validated through comparison with estimates of annual NCP derived from more complex labor-intensive methods such as Ar/O_2 ratios [*Quay et al.*, 2012; *Luz and Barkan*, 2009] and an independent method using measurements of DIC concentrations. We found no trend in the magnitude of the mean annual NCP over a 35° range in latitude. The contrast in the latitudinal variation of NCP derived from global circulation models and some satellite-derived models on the one hand, and NCP derived from in situ measurements on the other hand, highlights the need for improved global coverage of in situ data and an improved mechanistic understanding of why the two approaches differ. The method developed here is ideally suited to provide the required global coverage of in situ NCP data.

References

Aanderaa Data Instruments (2007), Operating manual oxygen optode.

Bates, N., M. Best, and D. Hansell (2005), Spatio-temporal distribution of dissolved inorganic carbon and net community production in the Chukchi and Beaufort Seas, *Deep Sea Res., Part II*, *52*(24–26), 3303–3323, doi:10.1016/j.dsr2.2005.10.005.

Behrenfeld, M., and P. G. Falkowski (1997), A consumer's guide to phytoplankton primary productivity models, *Limnol. Oceanogr.*, *42*(7), 1479–1491, doi:10.4319/lo.1997.42.7.1479.

Benson, B. B., and D. Krause (1984), The concentration and isotopic fractionation of oxygen dissolved in freshwater and seawater in equilibrium with the atmosphere, *Limnol. Oceanogr.*, *29*(3), 620–632, doi:10.4319/lo.1984.29.3.0620.

Boyer, T., M. Conkright, and S. Levitus (1999), Seasonal variability of dissolved oxygen, percent oxygen saturation, and apparent oxygen utilization in the Atlantic and Pacific Oceans, *Deep Sea Res., Part I*, *46*, 1593–1613.

Cianca, A., R. Santana, S. Hartman, J. Martin-Gonzalez, M. Gonzalez-Davila, M. Rueda, O. Linas, and S. Neuer (2013), Oxygen dynamics in the North Atlantic subtropical gyre, *Deep Sea Res., Part II*, *93*, 135–147, doi:10.1016/j.dsr2.2013.01.004.

Cooper, D., A. Watson, and R. Ling (1998), Variation of pCO2 along a North Atlantic shipping route (UK to the Caribbean): A year of automated observations, *Mar. Chem.*, *60*(1–2), 147–164.

del Giorgio, P. A., and P. J. L. B. Williams (2005), *Respiration in Aquatic Ecosystems*, Oxford Univ. Press, New York.

Dickson, A., C. Sabine, and J. Christian (2007), *Guide to Best Practices for Ocean CO2 Measurements, PICES Spec. Publ. 3*, 176 pp., North Pacific Marine Science Organization, Sidney, B. C., Canada.

Ducklow, H., C. Carlson, and N. Bates (1995), Dissolved organic carbon as a component of the biological pump in the North Atlantic Ocean, *Philos. Trans. R. Soc. London, Ser. B, 348*, 161–167.

Ducklow, H. W., and S. C. Doney (2013), What is the metabolic state of the oligotrophic ocean? A debate, *Annu. Rev. Mar. Sci.*, *5*, 525–33, doi:10.1146/annurev-marine-121211-172331.

Emerson, S. (1987), Seasonal oxygen cycles and biological new production in surface waters of the subarctic Pacific Ocean, *J. Geophys. Res.*, *92*, 6535–6544.

Emerson, S. (2014), Annual net community production and the biological carbon flux in the ocean, *Global Biogeochem. Cycles*, *28*, 14–28, doi:10.1002/2013GB004680.

Emerson, S., and C. Stump (2010), Net biological oxygen production in the ocean—II: Remote in situ measurements of O_2 and N_2 in subarctic Pacific surface waters, *Deep Sea Res., Part I, 57*(10), 1255–1265, doi:10.1016/j.dsr.2010.06.001.

Emerson, S., P. Quay, D. Karl, C. Winn, L. Tupas, and M. Landry (1997), Experimental determination of the organic carbon flux from open-ocean surface waters, *Nature, 389*, 951–954.

Emerson, S., C. Stump, and D. Nicholson (2008), Net biological oxygen production in the ocean: Remote in situ measurements of O_2 and N_2 in surface waters, *Global Biogeochem. Cycles, 22*, GB3023, doi:10.1029/2007GB003095.

Emerson, S. R., and S. Bushinsky (2014), Oxygen concentrations and biological fluxes in the open ocean, *Oceanography, 27*(1), 168–171.

Falkowski, P. G. (1998), Biogeochemical controls and feedbacks on ocean primary production, *Science, 281*(5374), 200–206, doi:10.1126/science.281.5374.200.

García, H., and L. Gordon (1992), Oxygen solubility in seawater: Better fitting equations, *Limnol. Oceanogr., 37*(6), 1307–1312.

Garcia, H., and R. Keeling (2001), On the global oxygen anomaly and air-sea flux, *J. Geophys. Res., 106*, 31,155–31,166.

Garcia, H. E., R. A. Locarnini, T. P. Boyer, J. I. Antonov, O. K. Baranova, M. M. Zweng, and D. R. Johnson (2010), World Ocean Atlas 2009 volume 3: Dissolved oxygen, apparent oxygen utilization, and oxygen saturation, in *NOAA Atlas NESDIS 70*, edited by S. Levitus, 344 pp., U.S. Government Printing Office, Washington, D. C.

Gloël, J. (2012), Triple oxygen isotopes and oxygen/argon ratio measurements to enhance coastal and open ocean production/respiration comparisons, PhD thesis, University of East Anglia, Norwich, U. K.

Glover, D., W. Jenkins, and S. Doney (2005), *Modeling Methods for Marine Science*, Cambridge Univ. Press, Cambridge, U. K.

Grasshoff, K., K. Kremling, and M. Ehrhardt (1999), *Methods of Seawater Analysis,* 3rd ed., Wiley, New York.

Gruber, N., C. D. Keeling, and N. R. Bates (2002), Interannual variability in the North Atlantic Ocean carbon sink, *Science, 298*(5602), 2374–2378, doi:10.1126/science.1077077.

Gruber, N., et al. (2009), Oceanic sources, sinks, and transport of atmospheric CO_2, *Global Biogeochem. Cycles, 23*, GB1005, doi:10.1029/2008GB003349.

Hooker, S. B., N. W. Rees, and J. Aiken (2000), An objective methodology for identifying oceanic provinces, *Prog. Oceanogr., 45*, 313–338.

Johnson, K. (2010), Simultaneous measurements of nitrate, oxygen, and carbon dioxide on oceanographic moorings: Observing the Redfield ratio in real time, *Limnol. Oceanogr., 55*(2), 615–627.

Johnson, M. (2010), A numerical scheme to calculate temperature and salinity dependent air-water transfer velocities for any gas, *Ocean Sci., 6*, 913–932, doi:10.5194/os-6-913-2010.

Keeling, R., and B. Stephens (1998), Seasonal variations in the atmospheric O2/N2 ratio in relation to the kinetics of air-sea gas exchange, *Global Biogeochem. Cycles, 12*(1), 141–163.

Key, R. M., A. Kozyr, C. L. Sabine, K. Lee, R. Wanninkhof, J. L. Bullister, R. A. Feely, F. J. Millero, C. Mordy, and T.-H. Peng (2004), A global ocean carbon climatology: Results from Global Data Analysis Project (GLODAP), *Global Biogeochem. Cycles, 18*, GB4031, doi:10.1029/2004GB002247.

Körtzinger, A., J. Schimanski, and U. Send (2005), High quality oxygen measurements from profiling floats: A promising new technique, *J. Atmos. Oceanic Technol., 22*, 302–308.

Körtzinger, A., U. Send, R. S. Lampitt, S. Hartman, D. W. R. Wallace, J. Karstensen, M. G. Villagarcia, O. Llinás, and M. D. DeGrandpre (2008), The seasonal pCO_2 cycle at 49°N/16.5°W in the northeastern Atlantic Ocean and what it tells us about biological productivity, *J. Geophys. Res., 113*, C04020, doi:10.1029/2007JC004347.

Landschützer, P., N. Gruber, D. Bakker, and U. Schuster (2014), Recent variability of the global ocean carbon sink, *Global Biogeochem. Cycles, 28*, 927–949, doi:10.1002/2014GB004853.

Laws, E. (1991), Photosynthetic quotients, new production and net community production in the open ocean, *Deep Sea Res., Part A, 38*(1), 143–167.

Lee, K. (2001), Global net community production estimated from the annual cycle of surface water total dissolved inorganic carbon, *Limnol. Oceanogr., 46*(6), 1287–1297, doi:10.4319/lo.2001.46.6.1287.

Lefèvre, D., C. Guigue, and I. Obernosterer (2008), The metabolic balance at two contrasting sites in the Southern Ocean: The iron-fertilized Kerguelen area and HNLC waters, *Deep Sea Res., Part II, 55*, 766–776, doi:10.1016/j.dsr2.2007.12.006.

Lefèvre, N., and L. Merlivat (2012), Carbon and oxygen net community production in the eastern tropical Atlantic estimated from a moored buoy, *Global Biogeochem. Cycles, 26*, GB1009, doi:10.1029/2010GB004018.

Liang, J.-H., C. Deutsch, J. C. McWilliams, B. Baschek, P. P. Sullivan, and D. Chiba (2013), Parameterizing bubble-mediated air-sea gas exchange and its effect on ocean ventilation, *Global Biogeochem. Cycles*, doi:10.1002/gbc.20080.

Longhurst, A. (2006), *Ecological Geography of the Sea, Ecol. Geog. of the Sea Ser.*, 2nd ed., 560 pp., Academic Press, San Diego, Calif.

Luz, B., and E. Barkan (2009), Net and gross oxygen production from O2/Ar, 17O/16O and 18O/16O ratios, *Aquat. Microb. Ecol., 56*(2–3), 133–145, doi:10.3354/ame01296.

Mathis, J. T., J. N. Cross, N. R. Bates, S. Bradley Moran, M. W. Lomas, C. W. Mordy, and P. J. Stabeno (2010), Seasonal distribution of dissolved inorganic carbon and net community production on the Bering Sea shelf, *Biogeosciences, 7*(5), 1769–1787, doi:10.5194/bg-7-1769-2010.

McKinley, G. (2000), Interannual variability of the air-sea flux of oxygen in the North Atlantic, *Geophys. Res. Lett., 27*(18), 2933–2936.

Menemenlis, D., J. Campin, P. Heimbach, C. Hill, T. Lee, A. Nguyen, M. Schodlok, and H. Zhang (2008), ECCO2: High resolution global ocean and sea ice data synthesis, *Mercator Ocean Q. Newsl., 31*, 13-21.

Mintrop, L. (2011), VINDTA manual for versions 3S and 3C.

Najjar, R. G., and R. Keeling (2000), Mean annual cycle of the air-sea oxygen flux: A global view, *Global Biogeochem. Cycles, 14*(2), 573–584.

Najjar, R. G., et al. (2007), Impact of circulation on export production, dissolved organic matter, and dissolved oxygen in the ocean: Results from Phase II of the Ocean Carbon-cycle Model Intercomparison Project (OCMIP-2), *Global Biogeochem. Cycles, 21*, GB3007, doi:10.1029/2006GB002857.

Neuer, S., et al. (2007), Biogeochemistry and hydrography in the eastern subtropical North Atlantic gyre. Results from the European time-series station ESTOC, *Prog. Oceanogr., 72*(1), 1–29, doi:10.1016/j.pocean.2006.08.001.

Quay, P., C. Peacock, K. Björkman, and D. Karl (2010), Measuring primary production rates in the ocean: Enigmatic results between incubation and non-incubation methods at Station ALOHA, *Global Biogeochem. Cycles, 24*, GB3014, doi:10.1029/2009GB003665.

Quay, P., J. Stutsman, and T. Steinhoff (2012), Primary production and carbon export rates across the subpolar N. Atlantic Ocean basin based on triple oxygen isotope and dissolved O_2 and Ar gas measurements, *Global Biogeochem. Cycles, 26*, GB2003, doi:10.1029/2010GB004003.

Redfield, A. (1963), The influence of organisms on the composition of sea-water, in *The Sea*, edited by M. N. Hill, pp. 26–77, Wiley-Interscience, New York.

Robinson, C., et al. (2006), The Atlantic Meridional Transect (AMT) programme: A contextual view 1995–2005, *Deep Sea Res., Part II*, *53*(14–16), 1485–1515, doi:10.1016/j.dsr2.2006.05.015.

Sarmiento, J., and N. Gruber (2006), *Ocean Biogeochemical Dynamics*, Princeton Univ. Press, Princeton, N. J.

Schuster, U., and A. Watson (2007), A variable and decreasing sink for atmospheric CO_2 in the North Atlantic, *J. Geophys. Res.*, *112*, C11006, doi:10.1029/2006JC003941.

Schuster, U., et al. (2013), An assessment of the Atlantic and Arctic sea-air CO_2 fluxes, 1990–2009, *Biogeosciences*, *9*(8), 10,669–10,724, doi:10.5194/bg-10-607-2013.

Serret, P., E. Fernández, C. Robinson, E. Woodward, and V. Pérez (2006), Local production does not control the balance between plankton photosynthesis and respiration in the open Atlantic Ocean, *Deep Sea Res., Part II*, *53*(14–16), 1611–1628, doi:10.1016/j.dsr2.2006.05.017.

Serret, P., C. Robinson, E. Fernández, E. Teira, G. Tilstone, and V. Pérez (2009), Predicting plankton net community production in the Atlantic Ocean, *Deep Sea Res., Part II*, *56*(15), 941–953, doi:10.1016/j.dsr2.2008.10.006.

Sharqawy, M. (2010), Thermophysical properties of seawater: A review of existing correlations and data, *Desalin. Water Treat.*, *16*(10), 354–380.

Sokal, R., and F. Rohlf (1995), *Biometry: The Principles and Practice of Statistics in Biological Research,* 3rd ed., W. H. Freeman, New York.

Spitzer, W. S., and W. J. Jenkins (1989), Rates of vertical mixing, gas exchange and new production: Estimates from seasonal gas cycles in the upper ocean near Bermuda, *J. Mar. Res.*, *47*(1), 169–196, doi:10.1357/002224089785076370.

Stanley, R. H. R., W. J. Jenkins, D. E. Lott, and S. C. Doney (2009), Noble gas constraints on air-sea gas exchange and bubble fluxes, *J. Geophys. Res.*, *114*, C11020, doi:10.1029/2009JC005396.

Stoffelen, A. (1996), Error modelling of scatterometer, in-situ, and ECMWF model winds: A calibration refinement, *Tech. Rep. 93R.*, Neth. Meteorol. Inst., de Bilt, Netherlands.

Sverdrup, H. (1953), On conditions for the vernal blooming of phytoplankton, *J. Conseil.*, *18*, 87–295.

Takahashi, T. (2009), Climatological mean and decadal change in surface ocean pCO_2, and net sea-air CO_2 flux over the global oceans, *Deep Sea Res., Part II*, *56*(8–10), 554–577, doi:10.1016/j.dsr2.2008.12.009.

Takahashi, T., and S. Sutherland (2002), Global sea-air CO_2 flux based on climatological surface ocean pCO_2, and seasonal biological and temperature effects, *Deep Sea Res., Part II*, *49*, 1601–1622.

Uppala, S., et al. (2005), The ERA-40 re-analysis, *Q. J. R. Meteorol. Soc.*, *131*, 2961–3012.

von Allmen, P., D. Menemenlis, G. Spiers, and D. Bogucki (2009), Remote sensing of the mixed layer depth. [Available at http://ecco2.jpl.nasa.gov/meetings/2009/Allmen_MLDlidar.pdf.]

Wanninkhof, R., W. E. Asher, D. T. Ho, C. Sweeney, and W. R. McGillis (2009), Advances in quantifying air-sea gas exchange and environmental forcing*, *Annu. Rev. Mar. Sci.*, *1*(1), 213–244, doi:10.1146/annurev.marine.010908.163742.

Watson, A. J., et al. (2009), Tracking the variable North Atlantic sink for atmospheric CO_2, *Science*, *326*(5958), 1391–1393, doi:10.1126/science.1177394.

Williams, P. J. L. B. (1993), On the definition of plankton production terms, *ICES Mar. Sci. Symp.*, *197*, 9–19.

Williams, P. J. L. B., and N. Jenkinson (1982), A transportable microprocessor-controlled precise Winkler titration suitable for field station and shipboard use, *Limnol. Oceanogr.*, *27*, 576–584.

Williams, P. J. I. B., P. D. Quay, T. K. Westberry, and M. J. Behrenfeld (2013), The oligotrophic ocean is autotrophic, *Annu. Rev. Mar. Sci.*, *5*, 535–49, doi:10.1146/annurev-marine-121211-172335.

Winkler, L. (1888), Die Bestimmung des im Wasser gelösten Sauerstoffes, *Ber. Dtsch. Chem. Ges.*, *21*, 2843–2846.

Woolf, D. K., and S. A. Thorpe (1991), Bubbles and the air-sea exchange of gases in near-saturation conditions, *J. Mar. Res.*, *49*(3), 435–466.

Zhang, J.-Z., G. Berberian, and R. Wanninkhof (2002), Long-term storage of natural water samples for dissolved oxygen determination, *Water Res.*, *36*(16), 4165–4168.